Domain structure in epitaxial metastable zinc-blende $(GaAs)_{1-x}(Ge_2)_x(001)$ alloys

L. T. Romano, I. M. Robertson, J. E. Greene, and J. E. Sundgren*
Department of Materials Science, the Coordinated Science Laboratory, and the Materials Research Laboratory, University of Illinois, 1101 West Springfield Avenue, Urbana, Illinois 61801
(Received 18 May 1987)

Plane-view and cross-sectional transmission electron microscopy have been used to examine the structure of epitaxial metastable zinc-blende $(GaAs)_{1-x}(Ge_2)_x$ alloys grown by rf sputter deposition on GaAs(001) substrates. An analysis of bright-field and dark-field images obtained from both fundamental and superstructure reflections showed, in addition to (111) microtwins and $(a/2)\langle 110\rangle$ line dislocations, the existence of ordered antiphase regions. However, the domain boundaries were not composed of Ga—Ga and As—As antisite bonds, as in III-V films grown on group-IV substrates, but formed stochastically due to the presence of Ge in agreement with previously published theoretical growth kinetic models. The Ge-mediated boundaries were planar and gave rise to an additional contrast in dark-field images obtained with {002} superstructure reflections. From cross-sectional micrographs and plane-view images obtained with samples tilted away from the [001] zone axis, the antiphase regions were shown to extend primarily parallel to the growth direction but with random off-axis components weaving through the matrix. The spatial extent and number density of these domains increased with increasing Ge concentrations.

I. INTRODUCTION

Over the last several years, a variety of new epitaxial, thermodynamically metastable, substitutional, semiconductor alloys including $InSb_{1-x}Bi_x$,[1] $(GaAs)_{1-x}(Ge_2)_x$,[2] $(GaSb)_{1-x}(Ge_2)_x$,[3] $(GaSb)_{1-x}(Sn_2)_x$,[4] and $Ge_{1-x}Sn_x$ (Ref. 5) have been synthesized from the vapor phase and their physical properties investigated. A key feature in the growth of most of these metastable alloy systems is the use of low-energy (typically 25–100 eV) self-ion or inert-ion bombardment of the growing film in order to provide continuous collisional mixing of the upper one or two monolayers *during* deposition. Of particular interest have been the $(A^{III}B^{V})_{1-x}(C_2^{IV})_x$ alloys $(GaAs)_{1-x}(Ge_2)_x$ and $(GaSb)_{1-x}(Ge_2)_x$ which require the simultaneous nonisovalent substitution of Ge onto both cation and anion sites. Single crystals have been grown at compositions ranging across the pseudobinary phase digrams of both systems even though the maximum $A^{III}B^{V}C^{IV}$ mutual solid solubilities are less than $\sim 4\%$.[6] The Ge-based alloys, in particular, have been shown to exhibit good thermal and temporal stability due to the large kinetic barrier compared to the small thermodynamic driving force for phase separation.[3,7]

An interesting aspect of these materials has been the nature of both the long-range and short-range ordering in $(A^{III}B^{V})_{1-x}(C_2^{IV})_x$ alloys. Clearly, at some value of x, there must exist a transition in the long-range order parameter from that corresponding to zinc blende to one representative of diamond. In order to test various assumptions concerning the atomic arrangements incorporated into models[8,9] which were developed initially to explain optical-absorption measurements,[2] a combination of Raman scattering,[10,11] extended x-ray absorption fine structure (EXAFS),[12] high-resolution x-ray diffraction (HR-XRD),[13] and ion channeling[14] experiments have been carried out.

Raman spectra from $(GaSb)_{1-x}(Ge_2)_x$ exhibited a "one-two" type mode behavior.[10] The frequency of the GaSb-like longitudinal-optical phonon mode did not shift appreciably with x and there was evidence of a small transverse-optical phonon peak indicating a zinc-blende structure on the GaSb-rich side.[11] More importantly, the spectra showed no evidence for Sb-Sb pairs. (The Raman peak due to Ga-Ga pairs would have been obscured by the alloy peak.) EXAFS analyses indicated perfect short-range order, with no evidence of Ga—Ga bonds, throughout the entire composition range.[12] Long-range order in these alloys was also investigated using high-resolution triple-crystal XRD to measure the intensities of (400) fundamental and (200) superstructure reflections from $(GaSb)_{1-x}(Ge_2)_x$ as a function of x. A long-range order parameter S was determined from these results and found to decrease very rapidly toward zero near $x=0.3$.[13]

Growth kinetic models for $(A^{III}B^{V})_{1-x}(C_2^{IV})_x$ alloys have been published recently by Kim and Stern[15] and Davis and Holloway.[16] The two models involve computer simulations of film growth with slightly different selection rules. In both cases, perfect short-range order is preserved and a long-range ordering transition near $x=0.3$ is obtained for (100)-oriented film growth. In addition, both models provide some interesting insights predicting, for example, that the long-range order in these alloys should depend upon the substrate crystal orientation. Davis and Holloway also discuss the possibility of a unique type of antiphase (referenced to the cation and anion sublattice sites in the substrate) region

©1987 The American Physical Society

occurring in the film with no "wrong" (i.e., $A^{\rm III}$—$A^{\rm III}$ or $B^{\rm V}$—$B^{\rm V}$ bonds at the boundary due to the mediation of Ge.

In this paper we present the initial results of a transmission electron microscopy (TEM) study of the structure of metastable zinc-blende $(GaAs)_{1-x}(Ge_2)_x$ alloys grown by rf sputter deposition on GaAs(001) substrates. Specimens were examined in both bright field and dark field using fundamental and superstructure reflections. The TEM results showed that all films were epitaxial single crystals in which the primary defects with (111) microtwins. Plane-view and cross-sectional images obtained using both fundamental and superstructure reflections were used to establish the existence of Ge-mediated antiphase regions. Furthermore, by tilting the specimens along known crystallographic directions, with respect to the electron beam, the antiphase regions were shown to extend primarily parallel to the growth direction but with random off-axis components weaving through the matrix. The number density and spatial extent of the domains increased with increasing Ge concentration. These results appear to be in general agreement with the growth kinetics model of Davis and Holloway for (100)-oriented $(A^{\rm III}B^{\rm V})_{1-x}(C_2^{\rm IV})_x$ alloys.[16]

II. EXPERIMENTAL PROCEDURE

The $(GaAs)_{1-x}(Ge_2)_x$ films used in this study had compositions ranging from $x=0$ to 0.30 and were grown by rf sputter deposition on GaAs(001) substrates. The sputtering system has been described previously[4,17,18] and only the essential features are noted here. The system base pressure during these experiments was better than 10^{-7} Torr (10^{-5} Pa), while the pressure during deposition was dynamically maintained at 15 mTorr (2 Pa). Sputtering was carried out in Ar gas which had an initial purity of 99.999% and was further purified by passing it through a Ti sponge getter at 900 °C prior to introducing it into the growth chamber. The induced potential on the substrate, with respect to the positive space-charge region in the plasma, was −75 V.

The film growth procedure was similar to that used for $(GaSb)_{1-x}(Sn_2)_x$.[4] The source material for deposition was supplied by a series of composite GaAs/Ge targets which were fabricated from undoped single-crystal GaAs and Ge wafers. New targets were always sputter etched for ~10 h before initiating film growth experiments. The target voltage during sputtering was ~1200 V, corresponding to a deposition rate of approximately 1 μm h^{-1} for a target-to-substrate separation of 4 cm. The film growth temperature was 520 °C±20 °C. Excess As was supplied to the growing film by an effusion cell charged with pure As and maintained at 300 °C.

The substrates used in these experiments were undoped, semi-insulating, polished GaAs(001) wafers which were introduced into the growth chamber through a differentially-pumped sample load lock. Initial substrate preparation consisted of degreasing by successive rinses in trichloroethylene, acetone, methanol, and deionized water. The substrates were then blown dry in dry N_2, etched for 3 min in a 7:1 by volume solution of H_2SO_4:H_2O_2, and, without air exposure, rinsed in deionized water and again blown dry in N_2. Liquid In was used to provide a thermal contact between the substrate and the GaAs-coated Mo platen. Final substrate cleaning consisted of heating, in vacuum, to 600 °C for 5 min in order to desorb the oxide layer.

Film compositions of samples with thicknesses ≥1 μm were determined by energy dispersive analysis in a JEOL electron microprobe. Ge and GaAs single-crystal wafers were used as reference standards. Matrix corrections for x-ray fluorescence, absorption, and atomic number were carried out using the MAGIC V computer program.[19] The reported compositions are accurate to within ±1.0 at. %.

The films were examined by transmission electron microscopy in a Philips EM 420 instrument operated at 120 keV. Bright-field and dark-field images were obtained from both fundamental and {200} superstructure reflections. Electron transparent samples were prepared for plane-view observation by a multistep process. Disks, 3 mm in diameter, were cut from the samples using an ultrasonic disk cutter. The disk were then ground from the substrate side to a thickness of ~150 μm. Further thinning, to ~50 μm, was accomplished using 1-μm-diam diamond paste while electron transparency was achieved by Ar^+ ion milling at 100 K using a 5.5-kV, 0.5-mA cm^{-2} beam incident at an angle of 13°. Cross-sectional TEM (XTEM) specimens were prepared by first cutting the substrates into 3×5-mm^2 slabs and forming couples by gluing two slabs together with the film sides facing each other. Slices, ~1 mm wide, were cut from the glued couples with a diamond saw and the slices ground to a thickness of ~40 μm using 5-μm-diam Al_2O_3 powder. The thin slices were then glued to a Cu washer and further thinned from both sides using Ar^+ ion milling, as described above, until electron transparency was achieved.

III. RESULTS AND DISCUSSION

All samples examined were epitaxial single crystals with no evidence of either large-angle grain boundaries or second-phase precipitates. The alloys exhibited a zinc-blende structure, as indicated by the presence of {200} superstructure reflections in addition to the fundamental reflections. The intensities of the {200} reflections, however, were found to decrease rapidly with increasing Ge concentrations in films with x greater than ~0.2. This is in agreement with results from triple-crystal high-resolution x-ray diffraction measurements carried out on $(GaAs)_{1-x}(Ge_2)_x$ alloys grown on GaP(001) substrates by ultrahigh-vacuum (UHV) ion-beam sputter deposition.[20]

Figure 1(a) is a [100] zone-axis diffraction pattern, with the {220} fundamental and {200} superstructure reflections labeled, from a typical $(GaAs)_{0.80}(Ge_2)_{0.20}$ film. The (220) bright-field image in Fig. 1(b) shows a single-phase structure with the presence of $(a/2)\langle 110\rangle$ line dislocations and $(a/6)\langle 211\rangle$ partial dislocations. The faults bounded by the partial dislocations are invisible using this reflection. However, by examination of

images obtained with other reflections, the faults were determined to be (111) microtwins rather than isolated stacking faults. Contrast from the microtwins can be seen in the dark-field image, obtained using the (020) reflection, in Fig. 1(c). Scanning microchemical x-ray analyses in the TEM, carried out using an electron beam with a diameter of ~ 80 nm, indicated that the composition was uniform throughout the film.

A comparison of Figs. 1(b) and 1(c) also reveals another type of contrast in the form of domain boundaries separating regions both of which have a zinc-blende structure. Such boundaries were never observed in dark-field images taken from pure GaAs samples. The domain regions in $(GaAs)_{0.80}(Ge_2)_{0.20}$ were found to be randomly distributed and varied in in size from ~ 50 to 150 nm with the boundaries either forming closed loops or terminating at microtwins. The percentage of area enclosed within the boundaries increased only slightly, $\sim 2-3\,\%$, with increasing x between 0.10 and 0.20. However, samples grown with $x = 0.30$ exhibited a much higher number density of domains with greatly decreased sizes, < 50 nm. It was difficult to assign a domain number density for samples with $x = 0.30$ since the TEM images are projected views through the thickness of the foil and therefore the domains appear interwoven.

The structure and topology of the domains were investigated as a function of film thickness for $(GaAs)_{0.80}(Ge_2)_{0.20}$ films by following the change in the $\{200\}$ dark-field contrast of the domain boundaries as the samples were tilted from the [001] zone axis towards the [110] zones. Alloys with $x = 0.10$ and 0.30 were also studied, but the $x = 0.20$ alloy was found to provide a better sample for a detailed TEM investigation, since the domain density was higher than for $x = 0.10$ while individual domains were more easily imaged than in the $x = 0.30$ samples. Figure 2(a) shows part of a [001] stereographic projection on which the tilt positions used to obtain the images in Figs. 2(b)–2(d) are marked. As the sample was tilted away from the [001] zone, some parts of the boundaries became sharper and some broader, depending upon the image direction. For example, the right sides of domains A, B, and C were sharper when imaged near the [106] zone [Fig. 2(b)] than when imaged near the [001] zone axis [see Fig. 1(c)]. On the other hand, tilting towards the [102] zone resulted in a broadening of the upper right and the left sides of domain boundaries A, B, and C [compare Figs. 1(c) and 2(c)], while images taken near the $[0\bar{1}3]$ zone show a broadening of the upper and lower parts of the boundaries [compare Figs. 1(c) and 2(d)]. These results indicate that the boundaries are planar and surround a domain volume and that the domains extend primarily parallel to the [001] growth direction but have off-axis components that weave through the matrix.

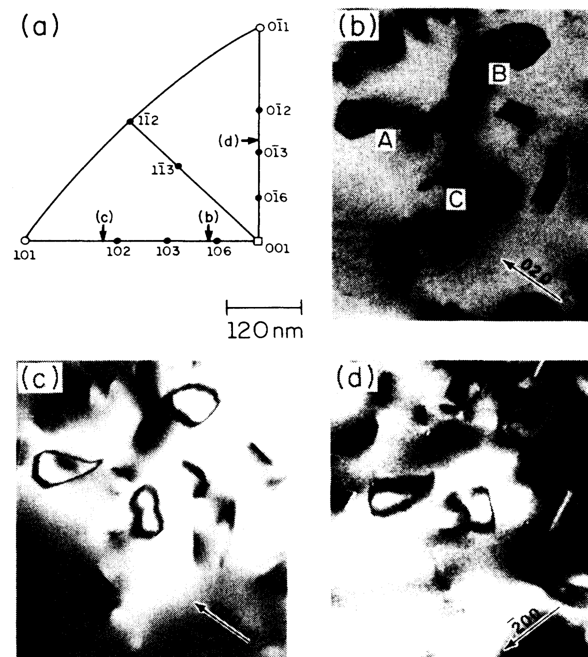

FIG. 2. (a) [001] stereographic projection showing the tilt positions used to obtain the $\{200\}$ dark-field images of $(GaAs)_{0.80}(Ge_2)_{0.20}$ shown in (b)–(d).

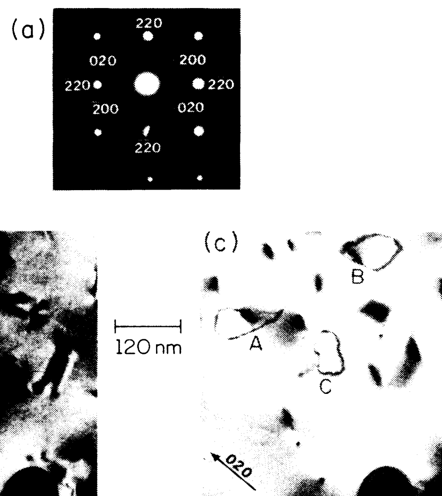

FIG. 1. (a) [001] zone-axis diffraction pattern, (b) (220) bright-field image, and (c) (020) dark-field image from a $(GaAs)_{0.80}(Ge_2)_{0.20}$ film.

The conclusions based on tilt experiment observations were confirmed by XTEM results. Figures 3(a) and 3(b) show XTEM dark-field images taken along a [110] zone axis using the (002) and $(00\bar{2})$ reflections, respectively. In both cases, the selected area diffraction aperture was centered at domain D. The micrographs show that the imaged domain has a columnarlike morphology and a width which broadens with increasing film thickness. It can also be seen that domain D undergoes essentially complete contrast reversal when the imaging conditions are changed from a (002) to a $(00\bar{2})$ reflection.

The contrast giving rise to the boundaries shown in the $\{002\}$ dark-field images presented above results from the formation of antiphase regions during film growth. Phase and antiphase regions are energetically degenerate

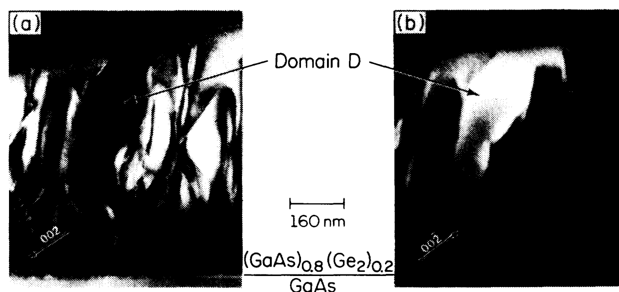

FIG. 3. (110) cross-sectional dark-field transmission electron micrographs from a $(GaAs)_{0.80}(Ge_2)_{0.20}$ film showing contrast reversal of antiphase domain D imaged using the (a) (002) and (b) $(00\bar{2})$ reflections.

in zinc-blende structures and simply related to each other by 180° rotations along any of the six ⟨110⟩ directions, as can be seen in the schematic diagram presented in Fig. 4. It should be noted that this is quite different than for most ordered metallic solid solutions where anitphase boundaries are describable by a lattice displacement across the boundary.[21] In the present case, the boundaries cannot be created or annihilated by the movement of dislocations.

Kuan and Chang[22] used multislice calculations[23] carried out with 64×256 beams to show that since the zinc-blende lattice does not have twofold rotational axes along the ⟨110⟩ directions, the amplitudes of (002) and $(00\bar{2})$ reflections from [110] projections will not be equal. This was later explained by Pond *et al.*[24] as being due to interference between the {002} and higher-order reflections. Thus, simultaneously imaging both zinc-blende phase and antiphase regions, using the (002) reflections, for example, is equivalent to imaging the phase region with the (002) and the antiphase region with the $(00\bar{2})$ reflection. It is this effect which gives rise to the contrast observed between the two regions in the zinc-blende structure. The amount of contrast observed depends upon the zone axis, i.e., the tilt condition, employed. For example, in the present results, Figs. 2(c) and 2(c), imaged near the [102] and $[0\bar{1}3]$ zone axes, respectively, show relatively little contrast, while Fig. 2(b), imaged near the [106] axis, exhibits significant contrast between phase and antiphase regions. The complete contrast reversal observed for domain D in Figs. 3(a) and 3(b) occurred due to the use of tilt conditions such that the higher-order reflection interference gave rise to a 180° phase change between the (002) and $(00\bar{2})$ images. Finally, in addition to the above effects, the presence of Ge provides further contrast at the phase-antiphase boundary as discussed below.

Antiphase boundaries have been observed in pure GaAs films grown on nonpolar diamond-structure substrates such as Ge(100) (Ref. 25) and Si(100) (Refs. 26 and 27) due to the lower symmetry of GaAs compared to Ge and the presence of demisteps of height $(\frac{1}{4})\langle 111\rangle$ in the surface of the diamond-structure substrate.[28] The resulting antisite Ga—Ga or As—As bonds which form along the boundary (see Fig. 4) represent high-energy defects in the structure. Antiphase boundaries have also been observed in III-V superlattice structures. Petroff *et al.*[29] reported that smooth films could not be obtained in thin $Ge/Ga_{1-x}Al_xAs$ superlattices. Instead, the films tended to grow in a columnar structure. Phillips[30] later proposed that this columnar growth morphology was due to the formation of antiphase domains in the $Ga_{1-x}Al_xAs$ layers with Ge segregating along the boundaries to reduce the energy associated with the antisite bonds and elastic strain fields.

In $(A^{\mathrm{III}}B^{\mathrm{V}})_{1-x}(C_2^{\mathrm{IV}})_x$ alloys such as $(GaAs)_{1-x}(Ge_2)_x$, antiphase boundaries form stochastically during growth, due to the presence of Ge. This is shown schematically in Fig. 5. The boundaries in this case, however, are not formed by Ga—Ga and As—As antisite bonds but by the mediation of Ge atoms. This gives rise to an additional contrast since the antiphase

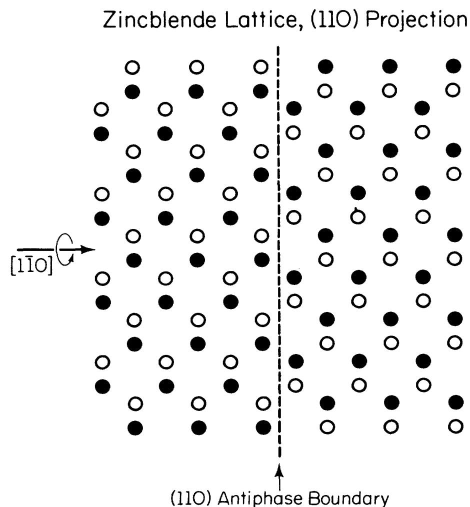

FIG. 4. Schematic diagram illustrating the relationship between phase and antiphase regions in the zinc-blende structure.

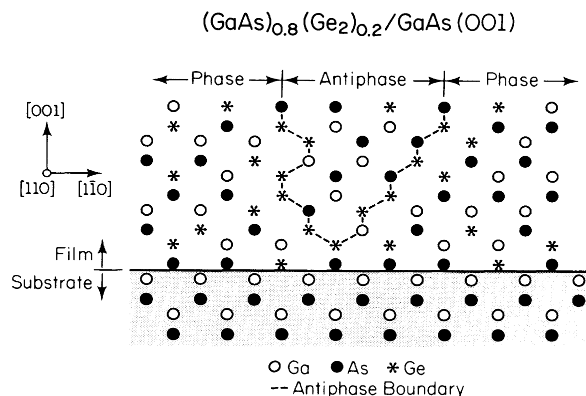

FIG. 5. Schematic diagram showing the formation of a Ge-mediated antiphase domain in $(GaAs)_{1-x}(Ge_2)_x$.

boundaries in this case are essentially two-dimensional Ge lattices with no zinc-blende ordering. Thus the {002} dark-field images would be expected to show boundaries with an intensity which is always lower than the zinc-blende phase and antiphase regions irrespective of the tilt. However, in certain tilts, parts of the boundary will disappear if they are perpendicular to the (002) diffraction vector. An example is given in Fig. 6 showing domain A at a higher magnification. This image was taken near the $[0\bar{1}5]$ zone with the [200] diffraction vector. A segment of the boundary, indicated by the arrow, was not visible at this tilt.

The amount of Ge necessary to populate the domain boundaries in a sample with $x=0.20$ was estimated from the average size and number density of the domains observed in the TEM to be only ≈ 0.1 at. %. Thus the domain boundaries have no significant effect on the average film composition. The absence of $A^{\rm III}$—$A^{\rm III}$ and $B^{\rm V}$—$B^{\rm V}$ bonds due to the mediation of Ge atoms is also consistent with previous EXAFS and Raman results on $(A^{\rm III}B^{\rm V})_{1-x}(C_2^{\rm IV})_x$ alloys.[10–12]

Finally, it should be pointed out that since the formation of Ge-mediated antiphase domain boundaries is stochastic, the frequency of domain initiation will be related to both the total number of Ge atoms impinging on the growth surface and the Ge adatom surface mobility. The latter is a function of growth conditions such as substrate temperature, growth rate, and ion irradiation conditions as well as the crystallographic orientation of the growth plane. Thus the average domain size and number density would be expected to be a function of the Ge concentration in the film, as observed in these experiments, and the film growth conditions, even when x is maintained constant. The effect of film orientation on domain structure has been demonstrated recently by Davis and Holloway[16,31] using computer simulations of both (100)- and (111)-oriented growth of $(A^{\rm III}B^{\rm V})_{1-x}(C_2^{\rm IV})_x$ alloys.

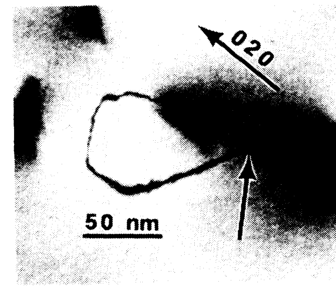

FIG. 6. Higher magnification (200) dark-field image of domain A (see Fig. 2) taken near the $[0\bar{1}5]$ zone.

ACKNOWLEDGMENTS

The authors gratefully acknowledge stimulating conversations with L. C. Davis (Ford Research) and K. E. Neumann and J. D. Dow (Notre Dame University) as well as the financial support of the Materials Science Division of the U.S. Department of Energy (DOE) under contract No. DE-AC02-76ER01198. We also appreciate the use of the facilities of the Center for Microanalysis, which is partially supported by the DOE, at the University of Illinois.

*Permanent address: Department of Physics and Measurement Technology, Linköping University, S-581 83 Linköping, Sweden.

[1]J. L. Zilko and J. E. Greene, J. Appl. Phys. **51**, 1549 (1980); **51**, 1560 (1980).

[2]S. A. Barnett, M. A. Ray, A. Lastras, B. Kramer, J. E. Greene, P. M. Raccah, and L. L. Abels, Electron. Lett. **81**, 891 (1982).

[3]K. C. Cadien, A. H. Eltoukhy, and J. E. Greene, Appl. Phys. Lett. **38**, 773 (1981); Vacuum **31**, 253 (1981).

[4]L. Romano, J. E. Sundgren, S. A. Barnett, and J. E. Greene, Superlatt. Microstruct. **2**, 233 (1986).

[5]S. I. Shah, J. E. Greene, L. L. Abels, Q. Yao, and P. M. Raccah, J. Cryst. Growth **83**, 3 (1987).

[6]S. I. Shah, K. C. Cadien, and J. E. Greene, J. Electron. Mater. **11**, 53 (1982); L. Romano, S. Fang, S. A. Barnett, and J. E. Greene (unpublished).

[7]K. C. Cadien, B. C. Muddle, and J. E. Greene, J. Appl. Phys. **55**, 4177 (1984).

[8]K. E. Newman, A. Lastras-Martinez, B. Kramer, S. A. Barnett, M. A. Ray, J. D. Dow, J. E. Greene, and P. M. Raccah, Phys. Rev. Lett. **50**, 1466 (1983); K. E. Newman and J. D. Dow, Phys. Rev. B **27**, 7495 (1983).

[9]H. Holloway and L. C. Davis, Phys. Rev. Lett. **43**, 830 (1984).

[10]T. N. Krabach, N. Wada, M. V. Klein, K. C. Cadien, and J. E. Greene, Solid State Commun. **45**, 895 (1983).

[11]R. Beserman, J. E. Greene, M. V. Klein, T. N. Krabach, T. C. McGlinn, L. T. Romano, and S. I. Shah, *Physics of Semiconductors,* edited by J. D. Chadi and W. A. Harrison (Springer-Verlag, New York, 1985), Vol. 17.

[12]E. A. Stern, F. Ellis, K. Kim, L. Romano, S. I. Shah, and J. E. Greene, Phys. Rev. Lett. **54**, 905 (1985).

[13]S. I. Shah, B. Kramer, S. A. Barnett, and J. E. Greene, J. Appl. Phys. **59**, 1482 (1986).

[14]A. D. F. Kahn, J. A. Eades, L. T. Romano, S. I. Shah, and J. E. Greene, Phys. Rev. Lett. **58**, 682 (1987).

[15]K. Kim and E. A. Stern, Phys. Rev. B **32**, 1019 (1985).

[16]L. C. Davis and H. Holloway, Phys. Rev. B **35**, 2767 (1987).

[17]J. E. Greene, C. E. Wikersham, and J. L. Zilko, J. Appl. Phys. **47**, 2289 (1976).

[18]J. E. Greene and C. E. Wikersham, J. Appl. Phys. **47**, 3630 (1976).

[19]J. W. Colby, in *Advances in X-ray Analysis,* edited by G. Mallet, M. Fay, and M. Mueller (Plenum, New York, 1968).

[20]M. Ray and J. E. Greene (unpublished).

[21]J. W. Edington, *Interpretation of Transmission Electron Micrographics* (Philips, Eindhoven, 1975), Vol. 3.

[22]T. S. Kuan and C. A. Chang, J. Appl. Phys. **54**, 4408 (1983).

[23]P. Goodman and A. F. Moodie, Acta Crystallogr. Sect. A **30**, 280 (1974).

[24]R. C. Pond, J. P. Gowers, D. B. Holt, B. A. Joyce, J. M. Neave, and P. K. Larsen, *Materials Research Society Symposium Proceedings,* Pittsburgh, 1984, edited by J. E. E. Baglin, D. R. Campbell, and W. K. Chu (MRS, Pittsburgh, 1984)

Vol. 25, p. 273.
[25]T. S. Kuan, *Materials Research Society Symposium Proceedings,* Pittsburgh, 1984, edited by W. Krakow, D. Smith, and L. W. Hobbs (MRS, Pittsburgh, 1984), Vol. 31, p. 143.
[26]R. Fisher, H. Morkoç, D. A. Neumann, H. Zabel, C. Choi, N. Otsuka, M. Longerbone, and L. P. Erickson, J. Appl. Phys. **60**, 1640 (1986).
[27]See, for example, the discussion in R. Fisher, H. Morkog, D. A. Neumann, H. Zabel, C. Choi, N. Otsuka, M. Longerbone, and L. P. Ericson, J. Appl. Phys. **60**, 1640 (1986).
[28]R. C. Pond, J. P. Gowers, and B. A. Joyce, Surf. Sci. **152/152**, 1191 (1984).
[29]P. E. Petroff, A. C. Gossard, A. Savage, and W. Wiegmann, J. Cryst. Growth **46**, 172 (1979).
[30]J. C. Phillips, J. Vac. Sci. Technol. **19**, 545 (1981).
[31]H. Holloway and L. C. Davis, Phys. Rev. B **35**, 3823 (1987).

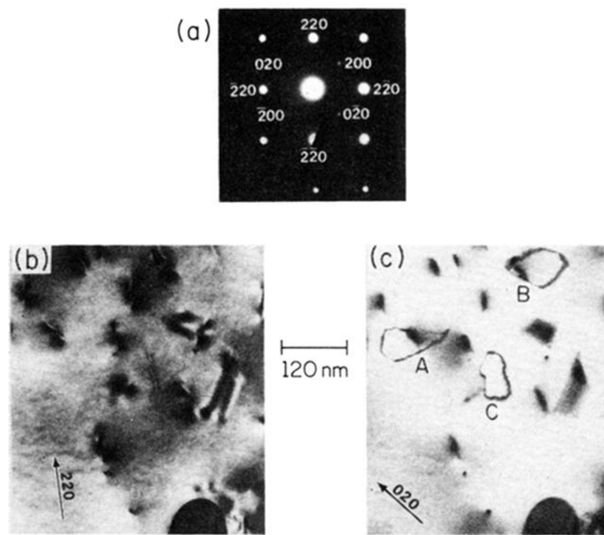

FIG. 1. (a) [001] zone-axis diffraction pattern, (b) (220) bright-field image, and (c) (020) dark-field image from a $(GaAs)_{0.80}(Ge_2)_{0.20}$ film.

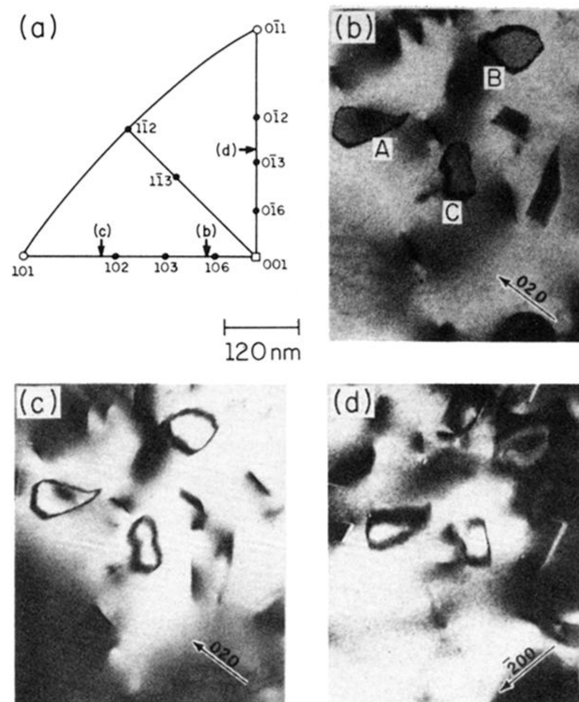

FIG. 2. (a) [001] stereographic projection showing the tilt positions used to obtain the {200} dark-field images of $(GaAs)_{0.80}(Ge_2)_{0.20}$ shown in (b)–(d).

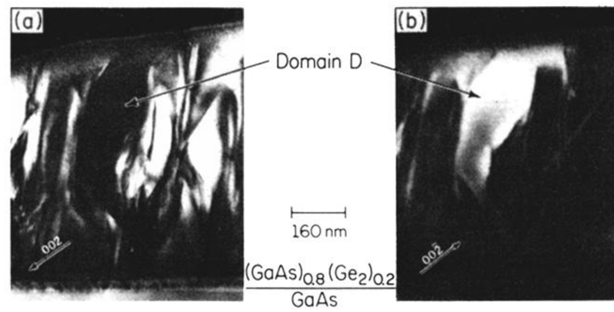

FIG. 3. (110) cross-sectional dark-field transmission electron micrographs from a $(GaAs)_{0.80}(Ge_2)_{0.20}$ film showing contrast reversal of antiphase domain *D* imaged using the (a) (002) and (b) $(00\bar{2})$ reflections.

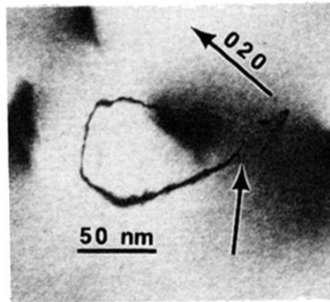

FIG. 6. Higher magnification (200) dark-field image of domain *A* (see Fig. 2) taken near the $[0\bar{1}5]$ zone.